Turning on Organic Radical Emitters

Matteo Dubbini,[†,‡] Federico Bonvini,[†,‡] Lorenzo Savi,[†] and Francesco Di Maiolo[*,†]

†*Department of Chemistry, Life Science and Environmental Sustainability, Università di Parma, 43124 Parma, Italy.*

‡*Contributed equally to this work*

E-mail: francesco.dimaiolo@unipr.it

Abstract

Radical emitters have attracted considerable interest because of their potential to surpass the limitations of singlet emitters due to spin statistics, thereby revolutionizing organic LEDs. Utilizing the well-known Pariser-Parr-Pople (PPP) model for correlated electrons in π-conjugated systems, we perform extended CISDT (XCISDT) calculations to explore the photophysics of various phenalenyl radicals differently decorated with nitrogen atoms. By introducing the PPP particle-hole difference operator and connecting it to DFT calculations, we offer a new tool for predicting highly emissive organic radicals using ground state quantum chemistry methods.

1 Introduction

Traditionally, organic light-emitting diodes (OLEDs) have used closed-shell organic molecules or phosphorescent materials to attain high electroluminescence efficiency. These devices typically depend on singlet or triplet exciton emission processes. Due to the singlet nature of the ground state, triplet excitons are non-emissive because of spin-conservation rules during

light-emission process. In first generation OLEDs, triplet excitons act as substantial energy sinks, thus restricting their internal quantum efficiency to a disappointing 25% due to spin statistics. To overcome this limitation, several approaches have been developed to make triplet excitons emissive, thereby enhancing the maximum internal efficiency of OLEDs to a satisfactory 100%. One strategy involves phosphorescent chromophores, where the inclusion of heavy metals promotes intersystem crossing.[1,2] Another strategy involves emitters that exhibit thermally activated delayed fluorescence (TADF),[3–11] as well as a combination of TADF and fluorescent systems used in hyperfluorescence OLEDs.[12] Additionally, multiresonant charge-transfer (MR-CT) emitters are also utilized.[13–24] On top of this, there has been a recent surge of interest in organic radicals as innovative emitters for OLED devices.[25–34] Organic radicals, characterized by their open-shell nature with one or more unpaired electrons, open the door to a new mechanism for light emission in OLEDs. Notably, organic radicals bypass singlet and triplet states, emitting light through transitions from a spin doublet excited state to a doublet ground state. This spin-allowed process eliminates the need for intersystem crossing, potentially resulting in higher quantum efficiencies since all recombination processes can contribute to light emission without substantial non-radiative losses.

The strong electron correlation potentially present in organic radicals complicates the calculation of their excited state properties. Consequently, employing quantum chemistry methods that can effectively handle the multiconfigurational nature of these electronic states becomes highly desirable. Among them, we mention multiconfigurational self-consistent field (MCSCF),[35] complete active space self-consistent field (CASSCF)[28,36,37] together with second-order perturbation theory (either CASPT2[38] or NEVPT2[34]), state-specific multireference perturbation theory (SSMRPT),[39] configuration interaction singles and doubles (CISD),[35] coupled cluster,[40,41] spin-flip restricted active space configuration interaction (SF-RASCI),[42–52] and complete active space configuration interaction density functional theory (CASCI-DFT).[53] However, the application of these methods has been confined to rather small systems. As

a result, conventional ground-state DFT and excited-state time-dependent DFT (TDDFT) methods remain attractive for studying organic radicals, despite the previously mentioned theoretical difficulties.[25–31,33,54–60] Due to the possible spin-contamination issues in the unrestricted version of TDDFT for open-shell molecules, explicitly spin-adapted TDDFT (X-TDDFT) is typically employed. Additionally, spin-polarized DFT calculations incorporating many-body perturbative corrections at the G_0W_0 level have also been utilized.[61]

We employ an alternative approach by conducting a comprehensive study of various phenalenyl radicals using the Pariser-Parr-Pople (PPP) model Hamiltonian to account for electron correlation in π-conjugated molecules. Developed in the 1950s,[62–64] this model has been successful in accurately describing the ground state and excited state properties of various small organic molecules.[63,65–74] The PPP model has recently made a comeback to address singlet-triplet (ST) inversion in some OLED emitters,[17,19,75] as well as doublet emission in both planar and non-planar organic radicals.[76,77] Although the PPP model was originally designed for π-conjugated hydrocarbons, it can be adapted to accommodate non-planar systems by incorporating additional terms that account for deviations from planarity.[74,77–81] Moreover, the model can be extended to systems containing heteroatoms by adjusting its key parameters against experimental data.[17,82–86] These adaptations significantly broaden the applicability of the PPP model, enabling its use in the study of strong radical emitters that are both non-planar and contain heteroatoms.[25–34]

An important symmetry inherent to the PPP model, but only approximately followed by more advanced (all-electron) Hamiltonians, is the so-called particle-hole (ph) symmetry. Alternant hydrocarbons provide a real molecular framework where this symmetry is closely approximated.[76,87–99] In such hydrocarbons, the carbon atoms can be divided into two distinct sets through a specific marking process: every other carbon atom is marked with a star, ensuring that no two starred carbons share a direct covalent bond. As a result, starred carbons only bond with unstarred carbons, and vice versa. Rings composed of an even number of atoms satisfy this condition, while rings with an odd number of atoms do

not (see SI Section S3 for examples of alternant and non-alternant hydrocarbons). The PPP particle-hole symmetry in alternant hydrocarbons is reflected in the unique arrangement of their orbital energy levels and the specific structure of the molecular orbitals (MOs). In alternant systems, MOs come in pairs with corresponding positive and negative energies. If the alternant system has an even number of atoms, the negative energy levels are fully occupied in the ground state, while the positive levels remain empty; thus, bonding and antibonding MOs appear as occupied-virtual pairs. Alternant hydrocarbons with an odd number of atoms have an additional feature, namely a singly occupied non-bonding orbital at zero energy (see SI Section S3). Finally, the particle-hole symmetry in the PPP model assumes the absence of heteroatoms. Therefore, when heteroatoms are introduced into the structure of an alternant hydrocarbon, they alter the energies of the bonding and antibonding molecular orbitals, resulting in an asymmetry among the energy levels.

In this work, we use the PPP model to investigate particle-hole symmetry breaking and its effect on doublet emission in several phenalenyl radicals differently decorated with nitrogen atoms. By comparing with PPP full-CI results, we demonstrate that triple excitations are necessary to accurately address both particle-hole symmetry breaking and doublet emission in organic radicals.

The objective of the PPP model is not to provide quantitatively accurate results for individual molecules.[19,100] Rather, PPP serves as a robust and simple method that, when applied to various molecular structures, reveals qualitative trends regarding the effects of electron correlation in π-conjugated molecules. The new insights obtained from this approach will help establish general and reliable guidelines for the rational design of novel organic radicals with strong doublet emission.

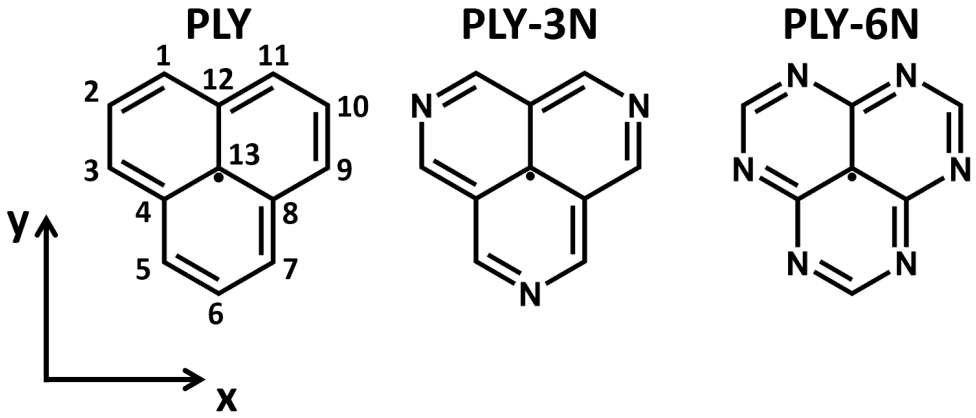

Figure 1: Molecular structures of three prototypical triangular organic radicals, namely phenalenyl (PLY), triazaphenalenyl (PLY-3N), and hexaazaphenalenyl (PLY-6N).

2 Methods

The PPP model is the most straightforward model for studying correlated electrons in π-conjugated molecules. Like the Hückel model, it only considers the $2p_z$ atomic orbitals (AOs) that are perpendicular to the molecular plane at each atomic site. However, unlike the Hückel model, the PPP model incorporates electron-electron (e-e) interactions using the zero differential overlap (ZDO) approximation, which ignores overlap integrals between $2p_z$ orbitals on different atoms. The PPP model Hamiltonian in the real-space (RS) atomic orbitals (AO) picture reads:

$$\begin{aligned}\hat{H}_{PPP} &= \sum_{\mu}\varepsilon_{\mu}\hat{n}_{\mu} - \sum_{\mu\nu,\nu>\mu}\sum_{\sigma} t_{\mu\nu}\left(\hat{a}^{\dagger}_{\mu\sigma}\hat{a}_{\nu\sigma} + \hat{a}^{\dagger}_{\nu\sigma}\hat{a}_{\mu\sigma}\right) \\ &\quad + \sum_{\mu} U_{\mu}\hat{n}_{\mu\uparrow}\hat{n}_{\mu\downarrow} + \sum_{\mu\nu,\nu>\mu} V_{\mu\nu}\left(Z_{\mu} - \hat{n}_{\mu}\right)\left(Z_{\nu} - \hat{n}_{\nu}\right) \end{aligned} \quad (1)$$

where $\hat{a}_{\mu,\sigma}$ and $\hat{a}^{\dagger}_{\mu,\sigma}$ annihilates and creates, respectively, an electron with spin σ on atom μ, and $\hat{n}_{\mu} = \sum_{\sigma}\hat{a}^{\dagger}_{\mu\sigma}\hat{a}_{\mu\sigma}$ counts the total number of electrons on site μ. The parameters in the first line of the Hamiltonian above are defined as follows: ε_{μ} is the on-site orbital energy, while $t_{\mu\nu}$ the hopping amplitude between atomic sites μ and ν. Specifically, in the PPP model, hopping is restricted to atoms connected by a σ-bond. The second line of the

Hamiltonian accounts for electron-electron interactions: U_μ represents the repulsion between two electrons on the same atom, $V_{\mu\nu}$ denotes the repulsion between electrons on different atoms, while Z_μ is the charge on site μ when π-electrons are removed ($Z_\mu = 1$ for both carbon and aza nitrogen atoms). We follow the Ohno expression for $V_{\mu\nu}$:[68,71,101]

$$V_{\mu\nu} = \frac{e^2}{4\pi\varepsilon_0} \Bigg/ \sqrt{r_{\mu\nu}^2 + \left(\frac{\varepsilon_r e^2}{4\pi\varepsilon_0 (U_\mu + U_\nu)}\right)^2} \tag{2}$$

where the relative dielectric constant ε_r is set to 2 to represent a typical organic medium.[71]

The RS PPP Hamiltonian is written on the basis that encompasses all possible states generated by distributing the n π-electrons among the N atoms. Specifically, the basis states are selected as eigenstates of the z-component spin operator $\hat{S}_z$. Accordingly, doublet states can be singled out by diagonalizing the PPP Hamiltonian in both $S_z = 0.5$ and $S_z = 1.5$ subspaces and looking for states that appear exclusively in the $S_z = 0.5$ subspace. Conversely, quartet states correspond to eigenstates that are present in both spin subspaces. As N grows, the size of the RS basis expands exponentially, reaching 2,944,656 states in the $S_z = 0.5$ subspace for the phenalenyl radicals in Fig. 1, leading to Hamiltonian matrices that are extremely large and sparse. First few eingestates and eigenvalues are derived using the implicitly restarted Lanczos algorithm as implemented in the ARPACK package.[102] This RS diagonalization yields full-CI results. To facilitate direct comparison with current quantum chemical techniques, we move to the MO picture of the PPP Hamiltonian. Specifically, in the mean-field Hartree-Fock (HF) approximation the PPP Hamiltonian in Eq. 1 boils down to the one-electron Fock operator:

$$\hat{\mathcal{F}}_{PPP} = \sum_\mu \left(\varepsilon_\mu + J_{\mu\mu} - K_{\mu\mu}\right) \hat{n}_\mu + \sum_{\mu\nu, \mu\neq\nu} \left(-t_{\mu\nu} - K_{\mu\nu}\right) \sum_\sigma \left(\hat{a}_{\mu\sigma}^\dagger \hat{a}_{\nu\sigma} + \hat{a}_{\nu\sigma}^\dagger \hat{a}_{\mu\sigma}\right) \tag{3}$$

In accordance with the PPP model, the ZDO approximation was utilized, resulting in a

diagonal Coulomb operator:

$$J_{\mu\mu} = \sum_{\lambda=1}^{N} (P_{\lambda\lambda} - Z_\lambda)\, V_{\lambda\mu} \tag{4}$$

while the exchange operator reads:

$$K_{\mu\nu} = (P_{\mu\nu}/2 - Z_\nu \delta_{\mu\nu})\, V_{\mu\nu} \tag{5}$$

In Eqs. 4 and 5 the density matrix elements are defined as :

$$P_{\mu\nu} = 2 \sum_{k=1}^{SOMO-1} c_{k\mu} c_{k\nu} + c_{SOMO,\mu} c_{SOMO,\nu} \tag{6}$$

where in the first term k runs on the doubly occupied MOs in the ground state configuration, while the second term accounts for the singly occupied MO (SOMO). $c_{k\mu}$ are the expansion coefficients of the k-th MO on the AOs (see SI, Section S1, Eqs. S1 and S2). The Fock operator above is addressed self-consistently through the variational principle. Typically, around 40 HF iterations are required to achieve convergence on the density matrix elements.

After obtaining the HF MOs for the ground state configuration $|g\rangle$, single, double, triple, and higher-order excited configurations are generated by transferring one, two, three, etc., electrons from occupied to virtual MOs.

The PPP Hamiltonian is subsequently expressed in the basis defined by the various configurations and diagonalized using the CI approach (see SI, Section S1). The PPP Hamiltonian in the CI basis is considerably less sparse than in the RS basis. However, the results converge rapidly with the number of excitations,[17,75] enabling the reliable analysis of excited states in phenalenyl radicals.

Molecular excited states $|f\rangle$ derived from the diagonalization of the CI Hamiltonian are employed to calculate optical spectra. The relevant electric dipole moment operator reads:

$$\hat{\vec{\mu}} = \hat{\mu}_x \vec{i} + \hat{\mu}_y \vec{j} = \sum_{\mu} (Z_\mu - \hat{n}_\mu)(x_\mu \vec{i} + y_\mu \vec{j}) \tag{7}$$

where x_μ, y_μ are site μ Cartesian coordinates in the molecular plane. Consequently, absorption spectra are obtained as:

$$A(\omega) \quad \propto \quad \omega \sum_f |\mu_{fg}|^2 \exp\left[\frac{(\omega - \omega_{fg})^2}{2\sigma^2}\right] \tag{8}$$

where the sum runs over the excited eigenstates, $\omega_{fg} = E_f - E_g$ is the relevant transition energy, and $\mu_{fg} = \langle f|\hat{\mu}|g\rangle$ is the transition dipole moment. We assigned a Gaussian bandshape ($\sigma = 0.1$ eV) to each transition. Transition energies and transition dipole moments enter the oscillator strength of the $|f\rangle \leftarrow |g\rangle$ transition:[103]

$$f_{fg} \quad = \quad \frac{2}{3}\frac{m_e}{\hbar e^2}\omega_{fg}|\mu_{fg}|^2 \tag{9}$$

where m_e is the electron mass and e the electron charge. Results presented in this study were obtained using an in-house PPP code in Fortran. This code extends the capabilities of the version introduced in Ref. 17 to handle open-shell systems.

3 Results & Discussion

3.1 PLY, PLY-3N and PLY-6N as playground systems

In this study, we begin by focusing on the three phenalenyl radicals depicted in Fig. 1. Phenalenyl (PLY) is an odd-alternant hydrocarbon with D_{3h} symmetry that has been extensively studied in its ground state using magnetic resonance techniques.[104–108] In contrast, little research on PLY has been conducted using optical spectroscopy, making it challenging to model its excited state properties. In Refs. 109,110, a weak absorption maximum at ∼2 eV is reported for PLY in MeTHF-ethanol mixture (7:1 v/v). When it comes to azaphenalenyls, experimental data are even scarcer, and relevant systems often need to be kinetically stabilized by bulky groups.[111–115] For instance, in Ref. 113, an absorption peak

slightly below 2 eV is observed for perchloro-2,5,8-triazaphenalenyl radical.

Fortunately, PPP parameters for carbon atoms are well-defined and transferable across various π-conjugated molecules.[63,68,71,116,117] Specifically, we set the carbon on-site energy to zero, use a standard on-site electron-electron interaction value of $U_C = 11.26$ eV, and a nearest-neighbor C-C hopping value of $t = -2.4$ eV. The situation is different for nitrogen atoms, as there is no universally accepted set of PPP parameters for them.[67–71,116,118–124] In this study, if not differently stated, we will use the aza nitrogen PPP parameters identified by Bedogni et al.[17] for 2T triangulenes, setting the on-site electron-electron repulsion to $U_N = 15.5$ eV and the site energy ε_N to -5 eV. The hopping integrals for C-N bonds were set to the same value as those for C-C bonds, a decision that has minimal impact on the results (see SI Section S2). For the molecular geometry, we set all bond angles to 120° and all bond lengths to 1.4 Å. Results for different geometries show only marginal differences, as detailed in SI Sections S2 and S5.

As outlined in Section 1, commonly used all-electron methods for organic radicals underscore the critical importance of accurately representing the potentially strong multiconfigurational nature of electronic states in these compounds. However, the rapid growth in the number of multiple excited configurations makes higher-order studies with all-electron methods impractical for large systems. In contrast, the PPP model, with its minimal active space, is particularly well-suited for examining the role of higher-order excited configurations in organic radicals. It is important to exercise caution when extending pure spin excited state theories from closed-shell systems to radicals, as the definition of excitation levels needs to be re-evaluated. Specifically, single excitations must be expanded to include double excitations which involve the simultaneous promotion of an α electron from the SOMO to virtual MOs and the promotion of a β electron from occupied MOs to the SOMO.[125] This leads to the spin pure extended CIS (XCIS) theory for the excited states of radicals.[77,125] The extension to higher order excitations leads to XCISD, XCISDT, etc. In the following we will always use the extended version of the corresponding CIs to preserve spin-purity.

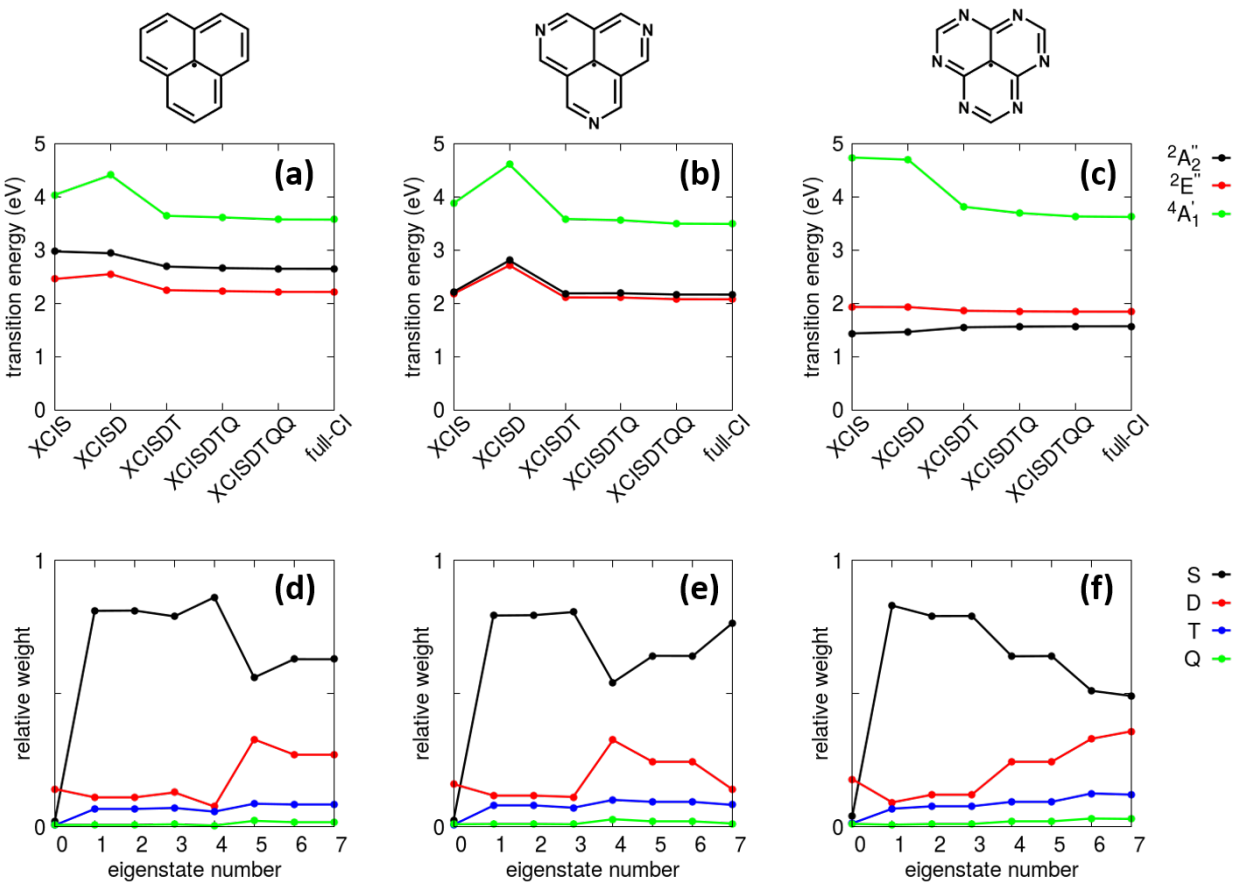

Figure 2: Excitation energies of the first few electronic states of PLY (panel a), PLY-3N (panel b), and PLY-6N (panel c) at various theoretical levels, together with the relative contributions of singly (S), doubly (D), triply (T), and quadruply (Q) excited configurations for the first seven doublet and quadruplet eigenstates of PLY (panel d), PLY-3N (panel e), and PLY-6N (panel f) calculated at the PPP-XCISDT level. Model parameters are specified in the main text.

The transition energies shown in Fig. 2a, b and c, demonstrate that truncating the expansion at the XCISD level stabilizes the ground state, but the stabilization of the excited states due to triple excitations is lacking. Consequently, XCISD overestimates transition energies, an error that is corrected when triply excited configurations are fully included, as also shown by the absolute energies in Fig.S5 in the SI, Section S4.

Panels d, e and f reveal the relative contributions of single (S), double (D), triple (T), and quadruple (Q) excitations in the lowest seven eigenstates of PLY, PLY-3N and PLY-6N. Singly and triply excited configurations have a negligible impact on the ground state

of the three molecules. In accordance with Brillouin's theorem, single and triple CIs do not directly mix with the ground state configuration, and their contribution is limited to indirect interactions with doubly excited configurations. In the first few excited states, the three molecules show double and triple excitations contributing similarly, around 10%. This finding aligns with our results for 2T triangulenes in Ref. 17 and indicates that a reliable approach to the excited states of these molecules should include not only double, but also triply excited configurations. Accordingly, given its balance between computational cost and accuracy, PPP-XCISDT was employed for the exploratory studies in this work. Comparison between PPP-XCISDT and ab initio CASSCF/CASPT2 results for PLY, PLY-3N, and PLY-6N is reported in the SI, Section S5.

Furthermore, Fig. 2 tells something more. In panel a, PLY lowest excited state is $^2E''$ and, since its ground state transforms as $^2A_1''$, the $^2E'' \leftarrow {}^2A_1''$ transition is allowed by point group symmetry. However, it is forbidden by particle-hole symmetry, so that the calculated transition dipole moment is null (see below). We note that the weak absorption maximum observed experimentally for PLY at approximately 2 eV[109,110] can be reproduced by incorporating inductive effects in the PPP model. Indeed, the PPP particle-hole symmetry can be relaxed by inductive effects[126] (see SI Section S6). PLY second excited doublet state is dark by point group symmetry, transforming as $^2A_2''$, and no effect of particle-hole symmetry breaking is expected. In panel b, the three aza nitrogens on the molecular rim stabilize the $^2A_2''$ dark state by $\sim$0.5 eV with respect to PLY. This effect is not observed for the $^2E''$ doublet, which, however, gains oscillator strength due to partial particle-hole symmetry breaking induced by doping with three nitrogen atoms on the molecular rim (as discussed below). In panel c, the six nitrogens stabilize the $^2A_2''$ dark state so much that it ends up below the doubly degenerate state, which remains almost at the same energy as in PLY and PLY-3N. In both PLY-3N and PLY-6N, the nitrogen atoms located on the rim play a more significant role in breaking particle-hole symmetry compared to the minor PPP on-site energy variations induced by inductive effects. Finally, in all three cases the first excited

quartet state $^4A_1'$ is always well above both $^2E''$ and $^2A_2''$ doublet excited states, being not appreciably affected by the increasing number of aza nitrogen atoms on the molecular rim.

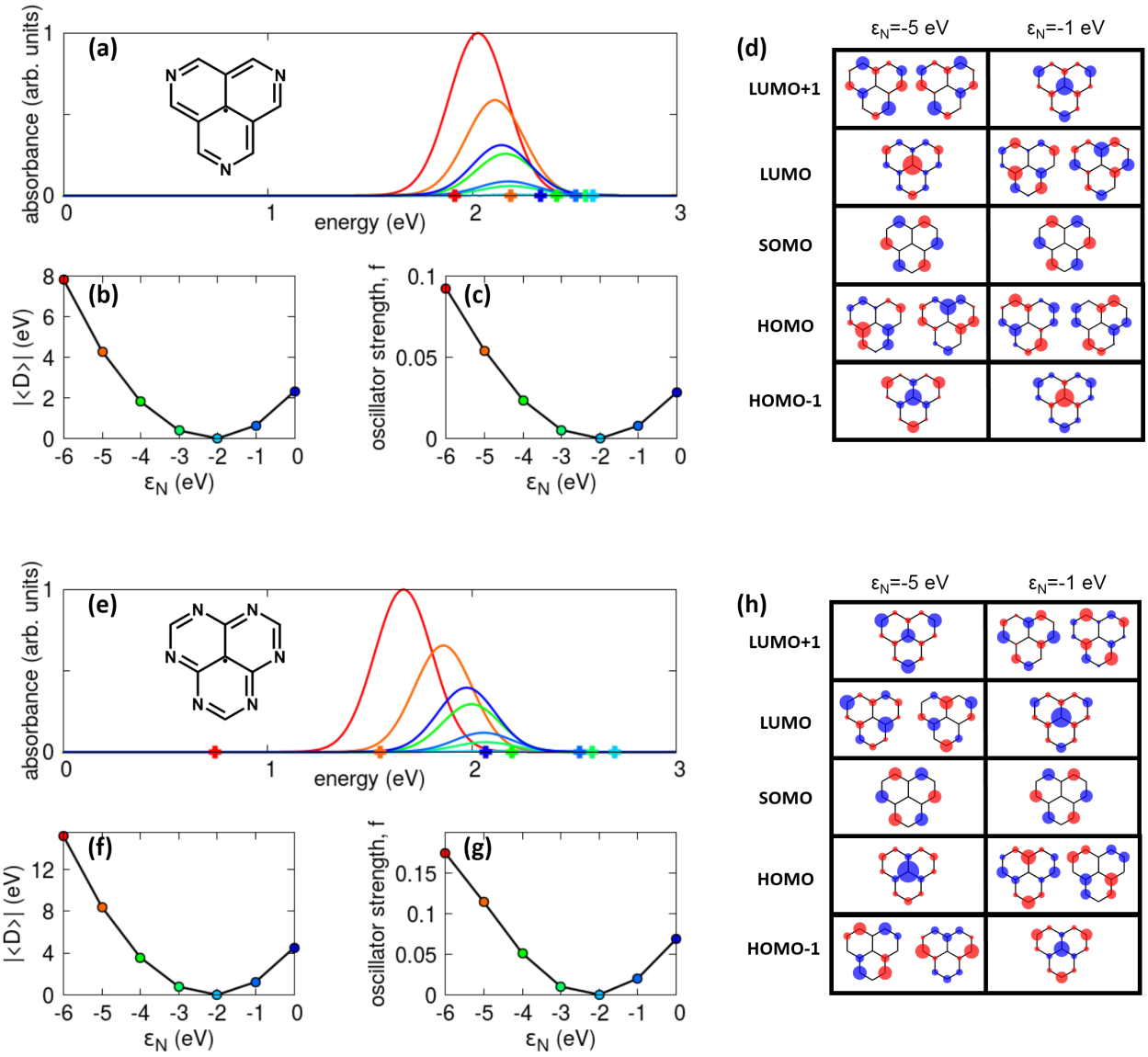

Figure 3: Particle-hole symmetry breaking effects on optical spectra of PLY-3N (panels a-d) and PLY-6N (panels e-h). (a) Absorption spectra of PLY-3N: colored lines show results for several ε_N values (same color code as in panels b and c), the crosses mark the position of the first dark doublet excited state. Calculated spectra are normalized to the maximum absorbance of the most intense spectrum; (b) Expectation value of the difference operator calculated on PLY-3N ground state for different ε_N values; (c) PLY-3N oscillator strength relevant to the first bright doublet excited state for different ε_N values; (d) PLY-3N frontier PPP-HF-MOs for two values of ε_N; (e) The same as (a) for PLY-6N; (f) The same as (b) for PLY-6N; (g) The same as (c) for PLY-6N; (h) The same as (d) for PLY-6N. All calculations performed at PPP-XCISDT level.

To better quantify particle-hole symmetry breaking, we introduce the difference operator, defined as the difference between the original PPP Hamiltonian in Eq. 1 and the PPP Hamiltonian transformed by particle-hole symmetry (see SI Section S7 for its derivation):

$$\hat{D} = \sum_{\mu} \left[U_{\mu} + 2\varepsilon_{\mu}\right] \left(\hat{n}_{\mu} - 1\right) \tag{10}$$

where the term in the square bracket is constant if there is no heteroatom in the system. The absolute value of the ground state expectation value $|\langle \hat{D} \rangle| = |\langle g|\hat{D}|g\rangle|$ is a direct measure of how much the particle-hole symmetry is broken, which in turn impacts the optical transition probabilities. In the following, we will see how $|\langle \hat{D} \rangle|$ changes as a function of the aza nitrogen PPP on-site energy in both PLY-3N and PLY-6N. The behavior observed for $|\langle \hat{D} \rangle|$ will be compared with the oscillator strength of the $^2E'' \leftarrow {}^2A_1''$ transition, as the lowest energy transition allowed by point group symmetry but forbidden by particle-hole symmetry.

In Fig. 3, panels a and e show spectra calculated at the PPP-XCISDT theory level, with the $^2A_2''$ dark doublet state indicated by a cross. Results are shown across a range of aza nitrogen PPP on-site energy values, ε_N, spanning from -6 eV to 0 eV, while keeping $U_N = 15.5$ eV. This range of energies encompasses scenarios from strongly electronegative nitrogen to a hypothetical situation where nitrogen electronegativity matches that of carbon, thus elucidating the role of nitrogen in these systems.

For PLY-3N (Fig. 3a), as the electron-withdrawing nature of the nitrogen increases (i.e., with more negative ε_N), both bright and dark states move first to the blue (ε_N going from 0 to -2 eV), and then red-shift for -6 eV $< \varepsilon_N <$ -3 eV, with the dark $^2A_2''$ doublet lying below the bright $^2E''$ state for $\varepsilon_N = -6$ eV. In panel b, the absolute value of the ground state expectation value of the particle-hole difference operator first decreases, reaching a minimum for $\varepsilon_N = -2$ eV, and then increases for further stabilization of the aza nitrogen orbital. Indeed, when $\varepsilon_N = -2$ eV the term in the square bracket in Eq. 10 is equal to 11.5 eV in the case of nitrogen atoms and to 11.26 eV for carbon atoms, thus making

minimal the particle-hole symmetry breaking as well as the oscillator strength of the $^2E''$ $\leftarrow$ $^2A_1''$ transition (see panel c). Moving away from $\varepsilon_N = -2$ eV, particle-hole symmetry is increasingly broken, $|\langle\hat{D}\rangle|$ increases, and the oscillator strength of the $^2E'' \leftarrow {}^2A_1''$ transition blows up.

Moving to PLY-6N (Fig. 3e), both dark and bright states again first blue-shift when the aza nitrogen PPP on-site energy is made more negative (i.e., $-2\text{eV} < \varepsilon_N < 0$), and then red-shift for ε_N going from -3 eV to -6 eV. Here, the dark $^2A_2''$ state lies below the bright one for $\varepsilon_N \leq -5$ eV. Similarly to PLY-3N, both $|\langle\hat{D}\rangle|$ (panel f) and oscillator strength of the $^2E'' \leftarrow {}^2A_1''$ transition (panel g) show a minimum for $\varepsilon_N = -2$ eV, increasing for either $\varepsilon_N \leq -3$ eV or $\varepsilon_N \geq -1$ eV.

The Hartree-Fock molecular orbitals of PLY-3N and PLY-6N, depicted in Fig. 3d and h, respectively, offer additional insights on the particle-hole symmetry breaking. PLY-3N shows a doubly degenerate HOMO within the ε_N range considered, while the roles of LUMO and LUMO+1 are reversed when increasing the electron-withdrawing character of the aza N atoms. In the case of PLY-6N, for increasingly negative ε_N values we have a change in the nature of HOMO and HOMO-1 as well as LUMO and LUMO+1. For comparison, the HF-MOs relevant to PLY are provided in SI Section S3. Unlike PLY-3N and PLY-6N, PLY exhibits energy levels that are symmetrically distributed above and below the SOMO.

The varying $|\langle\hat{D}\rangle|$ and oscillator strength behavior observed for PLY-3N and PLY-6N with changes in the aza nitrogen PPP site energy underscores the crucial role played by heteroatoms on the phenalenyl rim in breaking the particle-hole symmetry. Figure 4 illustrates $|\langle\hat{D}\rangle|$ and the oscillator strength dependence on the phenalenyl rim parameters, specifically ε_N and U_N. The green dot on the maps corresponds to the PLY parameters, where the rim is only composed of carbon atoms. If starting from this point we start decorating sites 2, 6, and 10 (cf. Fig. 1) with electron-withdrawing atoms, with progressively more negative on-site energy, the particle-hole symmetry breaking is strengthened as shown by increasingly larger values of the average difference operator. As a result, the color map on the right also shows

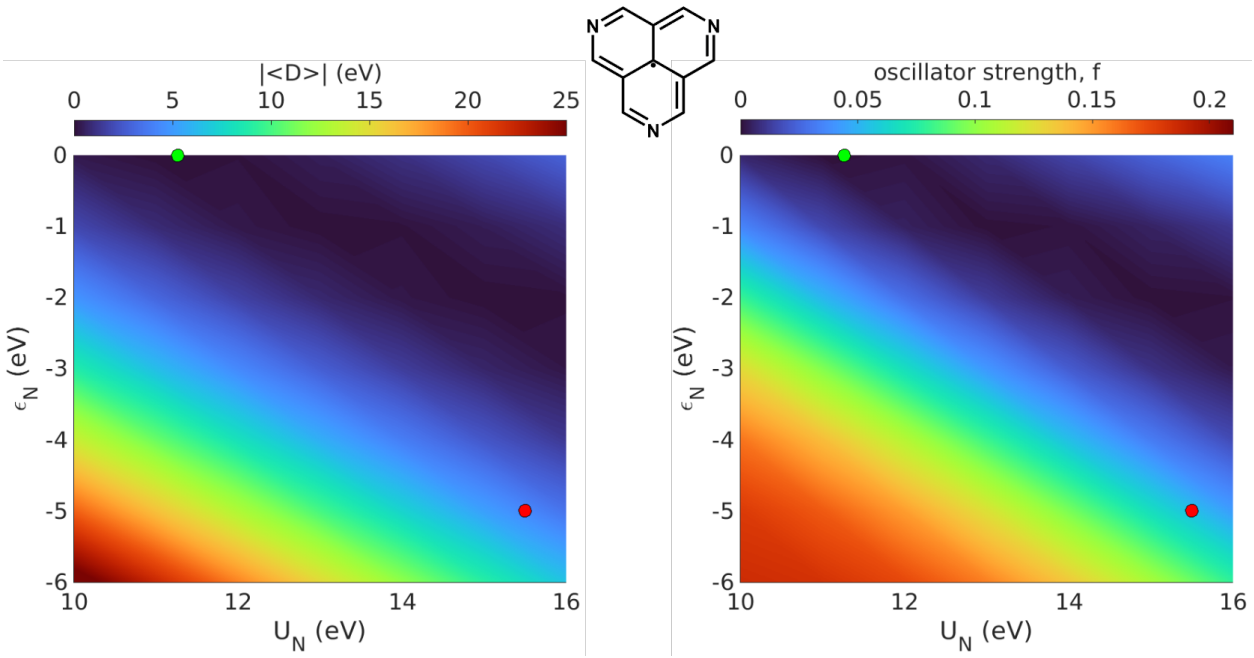

Figure 4: Left color map illustrates how $|\langle \hat{D} \rangle|$ varies with U_N and ε_N. Right color map reports how the oscillator strength of the transition ${}^2E'' \leftarrow {}^2A_1''$ depends on U_N and ε_N. In each map, the green dot indicates the parameters relevant to PLY, while the red dot those relevant to PLY-3N. Calculations performed at the PPP-XCISDT level, using the model parameters specified in the main text.

an increasing oscillator strength for the ${}^2E'' \leftarrow {}^2A_1''$ transition. However, upon increasing the on-site electron repulsion on sites 2, 6, and 10 from the value relevant to carbon atoms to that relevant to nitrogen atoms, the entity of the particle-hole symmetry breaking gets reduced. The red dot on the map corresponds to the parameters relevant to PLY-3N. For the sake of completeness, corresponding color maps obtained decorating sites 1, 3, 5, 7, 9, and 11 (cf. Fig. 1) with electron-withdrawing atoms are reported in the SI Section S8 and show a similar behavior.

3.2 Breaking the Symmetry: The Effect of Nitrogen Doping

The molecules discussed so far belong to the D_{3h} point group and have a low-energy dark doublet (${}^2A_2''$) state that gets stabilized by the increasing number of aza nitrogens on the molecular rim. In order to further investigate the rim role in phenalenyl radicals, we deco-

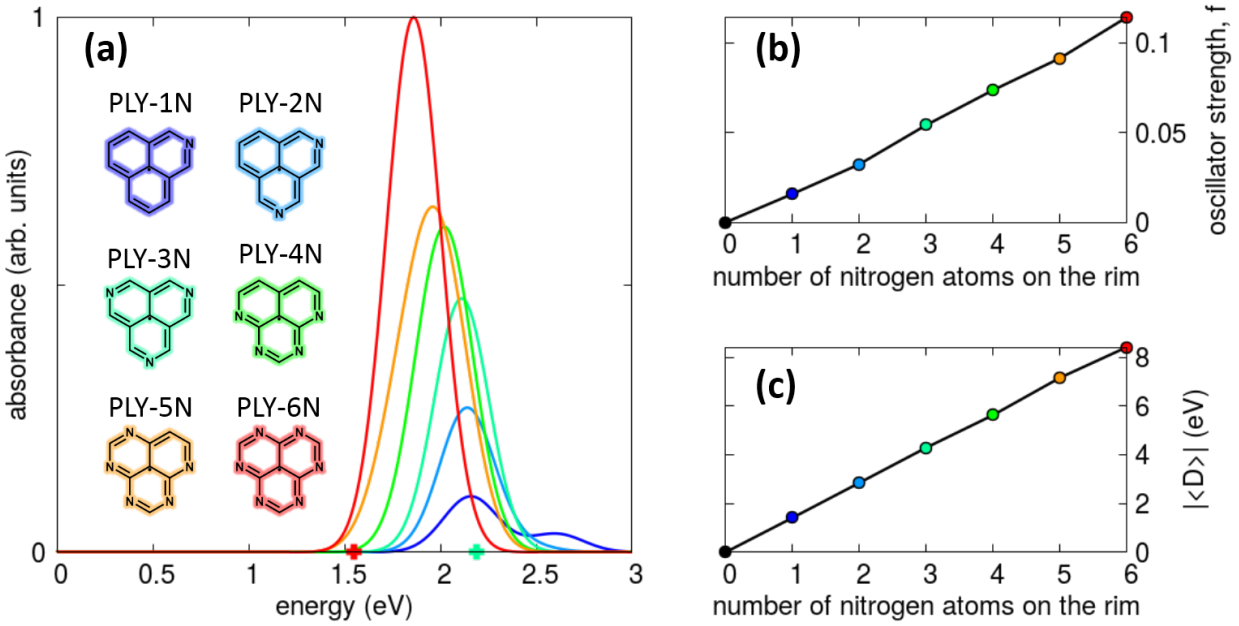

Figure 5: Decorating the rim of the phenalenyl radical with an increasing number of aza nitrogens. Calculated absorption spectra (panel a), oscillator strength integrated over the 0 eV - 3 eV spectral range (panel b), and absolute value of the ground state expectation value of the difference operator (panel c) for six different phenalenyls decorated with an increasing number of aza nitrogen atoms on the rim. In panel a, colored crosses mark the position of PLY-3N and PLY-6N first dark doublet state. In panel a, spectra are normalized to the maximum absorbance of the most intense spectrum. In panels b and c, a black dot is used for PLY results. Other parameters are defined in the main text. Calculations performed at the PPP-XCISDT theory level.

rated the external edge of PLY with an increasing number of aza nitrogen atoms, as shown in Fig. 5. All spectral features shift to the red as the number of N atoms on the external rim increases (see Fig. 5 panel a). The first dark ($^2A_2''$) doublet state shifts from ∼2.2 eV in PLY-3N to ∼1.5 eV in PLY-6N. When the molecular symmetry deviates from D_{3h}, the doublet dark state gains sizeable oscillator strength. A second weaker absorption peak appears at ∼2.6 eV in PLY-1N and gradually red-shifts when increasing the number of aza N atoms on the rim. Accordingly, in PLY-2N, PLY-4N and PLY-5N, the two absorption peaks observed in PLY-1N collapse into a single peak that moves to lower energies with the increasing number of aza N atoms. Quite interestingly, in PLY-1N a single aza nitrogen is already able to induce particle-hole symmetry breaking as also shown by a $|\langle\hat{D}\rangle|$ value of

$\sim$1.4 eV (panel c). By adding a second nitrogen atom as in PLY-2N, $|\langle\hat{D}\rangle|$ goes to $\sim$2.8 eV. By inspection of panel c, we see that each nitrogen atom contributes $\sim$1.4 eV to the $|\langle\hat{D}\rangle|$ value. Similar behavior is shown by the oscillator strength, with each aza N atom contributing $\sim$0.02 (panel b). Additional systems differently decorated with nitrogen atoms are shown in the SI Section S9.

Results discussed so far demonstrate the utility of the PPP model and $|\langle\hat{D}\rangle|$ in predicting radicals with significantly broken particle-hole symmetry as extremely promising doublet emitters for OLED with 100% internal quantum efficiency. Realistic (all-electron) hamiltonians do not strictly obey particle-hole symmetry, as it is only an approximate symmetry. The half-filled (i.e., one electron per site on average) PPP model inherently assumes particle-hole symmetry. The degree to which this symmetry is preserved in more advanced all-electron Hamiltonians depends on how closely the assumptions of the PPP model align with the specific system being studied. The degree to which particle-hole symmetry is preserved diminishes as these systems deviate from the idealized conditions assumed by the PPP model.

Looking back at the difference operator expression in Eq. 10, it relies on the on-site electron density, weighted by the repulsion between two electrons on the same atom (U_μ), plus twice the on-site energy (ε_μ). This calculation is then summed over the entire molecule. Therefore, we can consider whether $|\langle\hat{D}\rangle|$ can be determined using the total molecular energies obtained from quantum chemistry methods. Indeed, an effective molecular electron-electron repulsion energy U_{eff} can be estimated as the difference between the ionization potential and the electron affinity of the PLY radical,[127,128] $U_{eff} = E(PLY^-) + E(PLY^+) - 2E(PLY)$, where E is the DFT ground state radical total energy in the different oxidation states. Similarly, the effective on-site energy ε_{eff} can be obtained from the radical ionization potential as $\varepsilon_{eff} = E(PLY) - E(PLY^+)$, thus leading to the effective $|D|_{eff} = U_{eff} + 2\varepsilon_{eff}$. Of course, similar reasoning applies to other radicals as well. In Fig. 6, we compare $|\langle\hat{D}\rangle|$ calculated with respect to the PPP-XCISDT ground state and DFT ground state. If the quantitative agreement is far from perfect, the qualitative trend

is well reproduced, with $|\langle\hat{D}\rangle|$ increasing as the number of aza nitrogen atoms on the edge grows.

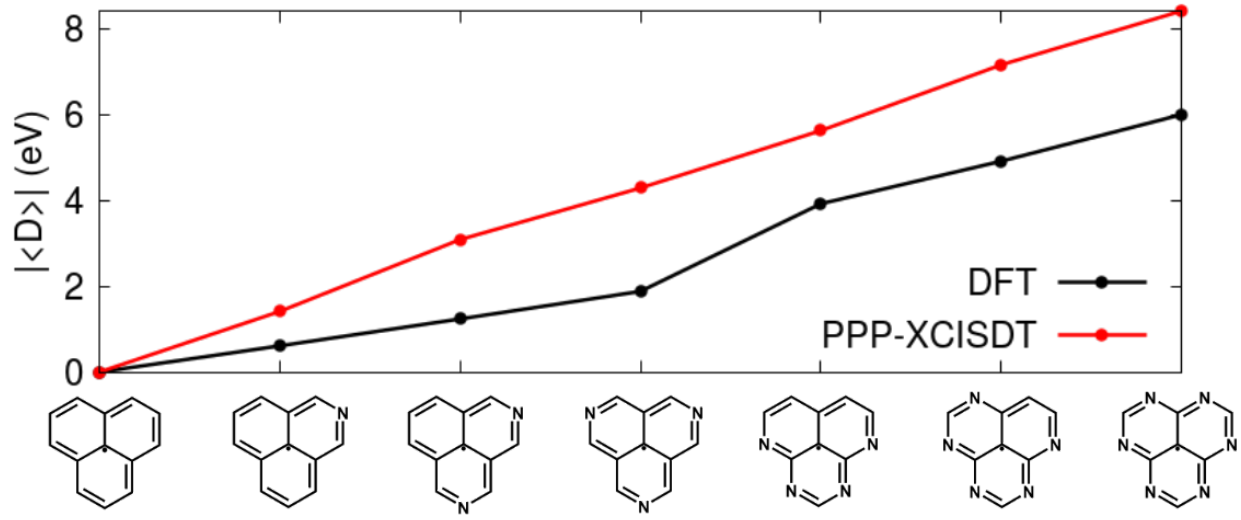

Figure 6: Particle-hole symmetry breaking in DFT and PPP. Ground state $|\langle\hat{D}\rangle|$ calculated for several phenalenyl radicals at DFT and PPP-XCISDT theory levels. PPP model parameters specified in the main text. DFT calculations performed using ROB3LYP functional with 6-31G(d,p) basis set as implemented in the Gaussian16 package,[129] and same regular geometry used for PPP calculations. DFT results were rescaled with respect to the value of $|\langle\hat{D}\rangle|$ relative to PLY, 6.77 eV.

4 Conclusions

Radical emitters have the potential to achieve 100% internal quantum efficiency in OLED applications, as their emission arises entirely from spin-allowed doublet-to-doublet transitions. This ensures that all generated excitons can contribute to light emission, unlike singlet emitters, which are constrained by exciton spin statistics. The emission color of doublet emitters can be precisely tuned through molecular design, necessitating computational studies to identify the most efficient species. However, from a theoretical perspective, strong electron correlation in these systems complicates the calculation of their excited state properties. Although multiconfigurational approaches are typically employed, their high computational cost makes them unsuitable for rapid screening and exploratory studies. Consequently, the

PPP model is a logical choice, offering a simple framework for describing interacting electrons in π-conjugated systems. Due to its simplicity, the PPP model is also well-suited for examining the impact of higher-order excited configurations on doublet emission. Moreover, since particle-hole symmetry is an exact symmetry of the PPP Hamiltonian, this model is ideal for studying its effect on the arrangement of radical MOs and the influence of chemical substitution. The PPP model, originally formulated for planar π-conjugated hydrocarbons, can be extended to non-planar systems through the inclusion of terms accounting for out-of-plane distortions. This expansion significantly enhances the versatility of the model, enabling its application to non-planar strong radical emitters.

Using PPP, in Fig. 2, we demonstrated that triply excited configurations are important for accurately addressing excited states of three prototypical phenalenyl radicals, namely PLY, PLY-3N, and PLY-6N. In PLY, the lowest optical transition is allowed by point group symmetry, but it is forbidden by particle-hole symmetry, thus making this molecule not fluorescent and of little interest for OLED applications. Upon rim doping with nitrogen atoms, the particle-hole symmetry gets destroyed and the $^2E'' \leftarrow ^2 A_1''$ transition becomes bright as in PLY-3N and PLY-6N. However, the aza nitrogens on the molecular edge also stabilize the $^2A_2''$ dark state. In the case of PLY-6N, the dark state energy stabilization is so strong that it ends up below the doubly degenerate state making the molecule not fluorescent.

To better quantify the entity of the particle-hole symmetry breaking, we introduced the difference operator $\hat{D}$ (cf. Eq. 10) as the difference between the original PPP hamiltonian and the particle-hole transformed one. In Figs. 3 and 4, we performed an exploratory study investigating the effect of nitrogen PPP on-site energy ε_N and electron-electron repulsion U_N on particle-hole symmetry breaking and doublet emission in PLY-3N and PLY-6N. In particular, strong particle-hole symmetry breaking can be obtained in the presence of heteroatoms where $U_\mu + 2\varepsilon_\mu$ significantly differs from that of carbon atoms.

In Fig. 5, starting from PLY, we decorated the edge with increasing number of nitrogen

atoms. Just a single heteroatom along the edge is sufficient to break particle-hole symmetry, resulting in $|\langle\hat{D}\rangle| = 1.4$ eV. Adding more nitrogen atoms amplifies this effect, with each additional nitrogen contributing approximately 1.4 eV to the total $|\langle\hat{D}\rangle|$ value. Similarly, the oscillator strength increases with each nitrogen atom, contributing around 0.02 to the overall value.

Triple excitations are computationally intensive, making their use in all-electron methods for exploratory studies challenging. However, our analysis indicates that the absolute value of the ground state average difference operator is already a reliable indicator of particle-hole symmetry breaking and finite oscillator strength. Although all-electron Hamiltonians do not follow particle-hole symmetry exactly, it is still possible to calculate an effective $|D|_{eff}$ by using ground state DFT molecular energies. In Fig. 6, we compared the ground state $|\langle\hat{D}\rangle|$ calculated at both the PPP and DFT levels for several phenalenyl radicals. We found a strong agreement between the two methods, paving the way for the use of ground state DFT in the search for new highly emissive organic radicals.

Data Availability Statement

The data that support the findings of this study are available from the corresponding author upon reasonable request.

Acknowledgement

We thank Matteo Bedogni and Prof. Anna Painelli for valuable discussions. We acknowledge financial support from Bando di ateneo per la ricerca 2023 - azione B. This work benefited from the equipment and framework of the COMP-R Initiative, funded by the *Departments of Excellence* program of the Italian Ministry for University and Research (MUR, 2023-2027) and from the support of the HPC (High Performance Computing) facility at the University of Parma. We acknowledge the CINECA award under the ISCRA initiative, for

the availability of high performance computing resources and support (project IsCb8_InveST (HP10CIDH42)). F.D.M. position was co-funded by the European Union - PON Research and Innovation 2014-2020.

Supporting Information Available

Electronic Supplementary Information (SI) available: Sec. S1 contains the PPP model in the Hartree-Fock approximation; Sec. S2 collects additional results obtained for different model parameters values as well as different molecular geometries (i.e., angles and bond lengths); Sec. S3 provides further details on alternant hydrocarbons and particle-hole symmetry; Sec. S4 deals with the effect of high order excitations on the ground state energy; Sec. S5 contains CASSCF and CASPT2 results for PLY, PLY-3N, and PLY-6N; Sec. S6 deals with the inductive effects in the PLY radical; Sec. S7 collects the difference operator derivation; Sec. S8 collects color maps obtained decorating sites 1, 3, 5, 7, 9, and 11 with electron-acceptor atoms; Sec. S9 collects results obtained for some additional nitrogen-decorated phenalenyl radicals.

References

(1) Baldo, M. A.; O'Brien, D. F.; You, Y.; Shoustikov, A.; Sibley, S.; Thompson, M. E.; Forrest, S. R. Highly efficient phosphorescent emission from organic electroluminescent devices. *Nature* **1998**, *395*, 151–154.

(2) Adachi, C.; Baldo, M. A.; Thompson, M. E.; Forrest, S. R. Nearly 100% internal phosphorescence efficiency in an organic light-emitting device. *Journal of Applied Physics* **2001**, *90*, 5048–5051.

(3) Yang, Z.; Mao, Z.; Xie, Z.; Zhang, Y.; Liu, S.; Zhao, J.; Xu, J.; Chi, Z.; Aldred, M. P.

Recent advances in organic thermally activated delayed fluorescence materials. *Chemical Society Reviews* **2017**, *46*, 915–1016.

(4) Liu, Y.; Li, C.; Ren, Z.; Yan, S.; Bryce, M. R. All-organic thermally activated delayed fluorescence materials for organic light-emitting diodes. *Nature Reviews Materials* **2018**, *3*, 18020.

(5) Shi, Y.-Z.; Wu, H.; Wang, K.; Yu, J.; Ou, X.-M.; Zhang, X.-H. Recent progress in thermally activated delayed fluorescence emitters for nondoped organic light-emitting diodes. *Chemical Science* **2022**, *13*, 3625–3651.

(6) Xiao, Y.; Wang, H.; Xie, Z.; Shen, M.; Huang, R.; Miao, Y.; Liu, G.; Yu, T.; Huang, W. NIR TADF emitters and OLEDs: challenges, progress, and perspectives. *Chemical Science* **2022**, *13*, 8906–8923.

(7) Li, B.; Liu, M.; Sang, L.; Li, Z.; Wan, X.; Zhang, Y. Role of the Intramolecular-Locking Strategy in the Construction of Organic Thermally Activated Delayed Fluorescence Emitters with Rotation-Restricted Acceptors. *Advanced Optical Materials* **2023**, *11*, 2202610.

(8) Olivier, Y.; Sancho-Garcia, J.-C.; Muccioli, L.; D'Avino, G.; Beljonne, D. Computational Design of Thermally Activated Delayed Fluorescence Materials: The Challenges Ahead. *The Journal of Physical Chemistry Letters* **2018**, *9*, 6149–6163.

(9) Northey, T.; Penfold, T. The intersystem crossing mechanism of an ultrapure blue organoboron emitter. *Organic Electronics* **2018**, *59*, 45–48.

(10) do Casal, M. T.; Veys, K.; Bousquet, M. H. E.; Escudero, D.; Jacquemin, D. First-Principles Calculations of Excited-State Decay Rate Constants in Organic Fluorophores. *The Journal of Physical Chemistry A* **2023**, 10033–10053.

(11) Di Maiolo, F.; Phan Huu, D. K. A.; Giavazzi, D.; Landi, A.; Racchi, O.; Painelli, A. Shedding light on thermally-activated delayed fluorescence. *Chemical Science* **2024**, *15*, 5434–5450.

(12) Stavrou, K.; Franca, L. G.; Danos, A.; Monkman, A. P. Key requirements for ultraefficient sensitization in hyperfluorescence organic light-emitting diodes. *Nature Photonics* **2024**, *18*, 554–561.

(13) Aizawa, N.; Pu, Y.-J.; Harabuchi, Y.; Nihonyanagi, A.; Ibuka, R.; Inuzuka, H.; Dhara, B.; Koyama, Y.; Nakayama, K.-i.; Maeda, S. et al. Delayed fluorescence from inverted singlet and triplet excited states. *Nature* **2022**, *609*, 502–506.

(14) Ehrmaier, J.; Rabe, E. J.; Pristash, S. R.; Corp, K. L.; Schlenker, C. W.; Sobolewski, A. L.; Domcke, W. Singlet–triplet inversion in heptazine and in polymeric carbon nitrides. *The Journal of Physical Chemistry A* **2019**, *123*, 8099–8108.

(15) Pollice, R.; Friederich, P.; Lavigne, C.; dos Passos Gomes, G.; Aspuru-Guzik, A. Organic molecules with inverted gaps between first excited singlet and triplet states and appreciable fluorescence rates. *Matter* **2021**, *4*, 1654–1682.

(16) Hall, D.; Sancho-García, J. C.; Pershin, A.; Ricci, G.; Beljonne, D.; Zysman-Colman, E.; Olivier, Y. Modeling of Multiresonant Thermally Activated Delayed Fluorescence EmittersProperly Accounting for Electron Correlation Is Key! *Journal of Chemical Theory and Computation* **2022**, *18*, 4903–4918.

(17) Bedogni, M.; Giavazzi, D.; Di Maiolo, F.; Painelli, A. Shining Light on Inverted Singlet–Triplet Emitters. *Journal of Chemical Theory and Computation* **2023**, *20*, 902–913.

(18) Omar, H.; Xie, X.; Troisi, A.; Padula, D. Identification of Unknown Inverted Singlet–Triplet Cores by High-Throughput Virtual Screening. *Journal of the American Chemical Society* **2023**, *145*, 19790–19799.

(19) Jorner, K.; Pollice, R.; Lavigne, C.; Aspuru-Guzik, A. Ultrafast Computational Screening of Molecules with Inverted Singlet–Triplet Energy Gaps Using the Pariser–Parr–Pople Semiempirical Quantum Chemistry Method. *The Journal of Physical Chemistry A* **2024**, *128*, 2445–2456.

(20) Barneschi, L.; Rotondi, L.; Padula, D. Molecular Geometry Impact on Deep Learning Predictions of Inverted Singlet–Triplet Gaps. *The Journal of Physical Chemistry A* **2024**, *128*, 2417–2426.

(21) Izu, A. E.; Matxain, J. M.; Casanova, D. Reverse intersystem crossing mechanisms in doped triangulenes. *Physical Chemistry Chemical Physics* **2024**, *26*, 11459–11468.

(22) Majumdar, A.; Ramakrishnan, R. Resilience of Hund's rule in the chemical space of small organic molecules. *Physical Chemistry Chemical Physics* **2024**, *26*, 14505–14513.

(23) Karak, P.; Manna, P.; Banerjee, A.; Ruud, K.; Chakrabarti, S. Reverse Intersystem Crossing Dynamics in Vibronically Modulated Inverted Singlet–Triplet Gap System: A Wigner Phase Space Study. *The Journal of Physical Chemistry Letters* **2024**, *15*, 7603–7609.

(24) Wilson, K. D.; Styers, W. H.; Wood, S. A.; Woods, R. C.; McMahon, R. J.; Liu, Z.; Yang, Y.; Garand, E. Spectroscopic Quantification of the Inverted Singlet–Triplet Gap in Pentaazaphenalene. *Journal of the American Chemical Society* **2024**, *146*, 15688–15692.

(25) Peng, Q.; Obolda, A.; Zhang, M.; Li, F. Organic Light-Emitting Diodes Using a Neutral π Radical as Emitter: The Emission from a Doublet. *Angewandte Chemie International Edition* **2015**, *54*, 7091–7095.

(26) Ai, X.; Evans, E. W.; Dong, S.; Gillett, A. J.; Guo, H.; Chen, Y.; Hele, T. J. H.; Friend, R. H.; Li, F. Efficient radical-based light-emitting diodes with doublet emission. *Nature* **2018**, *563*, 536–540.

(27) Kimura, S.; Tanushi, A.; Kusamoto, T.; Kochi, S.; Sato, T.; Nishihara, H. A luminescent organic radical with two pyridyl groups: high photostability and dual stimuli-responsive properties, with theoretical analyses of photophysical processes. *Chemical Science* **2018**, *9*, 1996–2007.

(28) Guo, H.; Peng, Q.; Chen, X.-K.; Gu, Q.; Dong, S.; Evans, E. W.; Gillett, A. J.; Ai, X.; Zhang, M.; Credgington, D. et al. High stability and luminescence efficiency in donor–acceptor neutral radicals not following the Aufbau principle. *Nature Materials* **2019**, *18*, 977–984.

(29) He, C.; Li, Z.; Lei, Y.; Zou, W.; Suo, B. Unraveling the Emission Mechanism of Radical-Based Organic Light-Emitting Diodes. *The Journal of Physical Chemistry Letters* **2019**, *10*, 574–580.

(30) Abdurahman, A.; Hele, T. J. H.; Gu, Q.; Zhang, J.; Peng, Q.; Zhang, M.; Friend, R. H.; Li, F.; Evans, E. W. Understanding the luminescent nature of organic radicals for efficient doublet emitters and pure-red light-emitting diodes. *Nature Materials* **2020**, *19*, 1224–1229.

(31) Cho, E.; Coropceanu, V.; Brédas, J.-L. Organic Neutral Radical Emitters: Impact of Chemical Substitution and Electronic-State Hybridization on the Luminescence Properties. *Journal of the American Chemical Society* **2020**, *142*, 17782–17786.

(32) Chen, Z.; Li, Y.; Huang, F. Persistent and Stable Organic Radicals: Design, Synthesis, and Applications. *Chem* **2021**, *7*, 288–332.

(33) Hudson, J. M.; Hele, T. J. H.; Evans, E. W. Efficient light-emitting diodes from organic radicals with doublet emission. *Journal of Applied Physics* **2021**, *129*, 180901.

(34) Gorgon, S.; Lv, K.; Grüne, J.; Drummond, B. H.; Myers, W. K.; Londi, G.; Ricci, G.; Valverde, D.; Tonnelé, C.; Murto, P. et al. Reversible spin-optical interface in luminescent organic radicals. *Nature* **2023**, *620*, 538–544.

(35) Vergés, J. A.; SanFabián, E.; Chiappe, G.; Louis, E. Fit of Pariser-Parr-Pople and Hubbard model Hamiltonians to charge and spin states of polycyclic aromatic hydrocarbons. *Physical Review B* **2010**, *81*, 085120.

(36) Marie, A.; Burton, H. G. A. Excited States, Symmetry Breaking, and Unphysical Solutions in State-Specific CASSCF Theory. *The Journal of Physical Chemistry A* **2023**, *127*, 4538–4552.

(37) Zhang, S.; Zhou, Z.; Qu, Z. Diradical-Based Strategy in Designing Narrowband Thermally Activated Delayed Fluorescence Molecules with Tunable Emission Wavelengths. *The Journal of Physical Chemistry Letters* **2024**, *15*, 2723–2731.

(38) Li, B.; Li, L.; Wang, Y.; Peng, J. CAS Calculation of the Excited States of the Methylthio Neutral Radical and Its Ions. *ACS Omega* **2020**, *5*, 24204–24210.

(39) Chattopadhyay, S.; Chaudhuri, R. K.; Mahapatra, U. S.; Ghosh, A.; Ray, S. S. State-specific multireference perturbation theory: development and present status. *WIREs Computational Molecular Science* **2016**, *6*, 266–291.

(40) Smith, C. E.; King, R. A.; Crawford, T. D. Coupled cluster methods including triple excitations for excited states of radicals. *The Journal of Chemical Physics* **2005**, *122*, 054110.

(41) Sengupta, A.; Ramabhadran, R. O.; Raghavachari, K. Breaking a bottleneck: Accurate extrapolation to "gold standard" CCSD(T) energies for large open shell organic radicals at reduced computational cost. *Journal of Computational Chemistry* **2015**, *37*, 286–295.

(42) Das, S.; Herng, T. S.; Zafra, J. L.; Burrezo, P. M.; Kitano, M.; Ishida, M.; Gopalakrishna, T. Y.; Hu, P.; Osuka, A.; Casado, J. et al. Fully Fused Quinoidal/Aromatic Carbazole Macrocycles with Poly-radical Characters. *Journal of the American Chemical Society* **2016**, *138*, 7782–7790.

(43) Huang, R.; Phan, H.; Herng, T. S.; Hu, P.; Zeng, W.; Dong, S.-q.; Das, S.; Shen, Y.; Ding, J.; Casanova, D. et al. Higher Order -Conjugated Polycyclic Hydrocarbons with Open-Shell Singlet Ground State: Nonazethrene versus Nonacene. *Journal of the American Chemical Society* **2016**, *138*, 10323–10330.

(44) Desroches, M.; Mayorga Burrezo, P.; Boismenu-Lavoie, J.; Peña Álvarez, M.; Gómez-García, C. J.; Matxain, J. M.; Casanova, D.; Morin, J.; Casado, J. Breaking Bonds and Forming Nanographene Diradicals with Pressure. *Angewandte Chemie International Edition* **2017**, *56*, 16212–16217.

(45) Lu, X.; Lee, S.; Hong, Y.; Phan, H.; Gopalakrishna, T. Y.; Herng, T. S.; Tanaka, T.; Sandoval-Salinas, M. E.; Zeng, W.; Ding, J. et al. Fluorenyl Based Macrocyclic Polyradicaloids. *Journal of the American Chemical Society* **2017**, *139*, 13173–13183.

(46) Liu, C.; Sandoval-Salinas, M. E.; Hong, Y.; Gopalakrishna, T. Y.; Phan, H.; Aratani, N.; Herng, T. S.; Ding, J.; Yamada, H.; Kim, D. et al. Macrocyclic Polyradicaloids with Unusual Super-ring Structure and Global Aromaticity. *Chem* **2018**, *4*, 1586–1595.

(47) Pérez-Guardiola, A.; Sandoval-Salinas, M. E.; Casanova, D.; San-Fabián, E.; Pérez-Jiménez, A. J.; Sancho-García, J. C. The role of topology in organic molecules: origin and comparison of the radical character in linear and cyclic oligoacenes and related oligomers. *Physical Chemistry Chemical Physics* **2018**, *20*, 7112–7124.

(48) Pérez-Guardiola, A.; Ortiz-Cano, R.; Sandoval-Salinas, M. E.; Fernández-Rossier, J.; Casanova, D.; Pérez-Jiménez, A. J.; Sancho-García, J. C. From cyclic nanorings to single-walled carbon nanotubes: disclosing the evolution of their electronic structure with the help of theoretical methods. *Physical Chemistry Chemical Physics* **2019**, *21*, 2547–2557.

(49) Ni, Y.; Sandoval-Salinas, M. E.; Tanaka, T.; Phan, H.; Herng, T. S.; Gopalakr-

ishna, T. Y.; Ding, J.; Osuka, A.; Casanova, D.; Wu, J. [n]Cyclo-para-biphenylmethine Polyradicaloids: [n]Annulene Analogs and Unusual Valence Tautomerization. *Chem* **2019**, *5*, 108–121.

(50) Sandoval-Salinas, M. E.; Carreras, A.; Casanova, D. Triangular graphene nanofragments: open-shell character and doping. *Physical Chemistry Chemical Physics* **2019**, *21*, 9069–9076.

(51) Casanova, D. Restricted active space configuration interaction methods for strong correlation: Recent developments. *WIREs Computational Molecular Science* **2022**, *12*, e1561.

(52) Preethalayam, P.; Roldao, J. C.; Castet, F.; Casanova, D.; Radenković, S.; Ottosson, H. 3,4-Dimethylenecyclobutene: A Building Block for Design of Macrocycles with Excited State Aromatic Low-Lying High-Spin States. *Chemistry – A European Journal* **2024**, *30*, e202303549.

(53) Ukai, T.; Nakata, K.; Yamanaka, S.; Kubo, T.; Morita, Y.; Takada, T.; Yamaguchi, K. CASCI-DFT study of the phenalenyl radical system. *Polyhedron* **2007**, *26*, 2313–2319.

(54) Morita, Y.; Kawai, J.; Fukui, K.; Nakazawa, S.; Sato, K.; Shiomi, D.; Takui, T.; Nakasuji, K. Topological Symmetry Control in Spin Density Distribution: Spin Chemistry of Phenalenyl-Based Neutral Monoradical Systems. *Organic Letters* **2003**, *5*, 3289–3291.

(55) Morita, Y.; Suzuki, S.; Sato, K.; Takui, T. Synthetic organic spin chemistry for structurally well-defined open-shell graphene fragments. *Nature Chemistry* **2011**, *3*, 197–204.

(56) Hattori, Y.; Kusamoto, T.; Nishihara, H. Luminescence, Stability, and Proton Response of an Open-Shell (3,5-Dichloro-4-pyridyl)bis(2,4,6-trichlorophenyl)methyl Radical. *Angewandte Chemie International Edition* **2014**, *53*, 11845–11848.

(57) Diez-Cabanes, V.; Seber, G.; Franco, C.; Bejarano, F.; Crivillers, N.; Mas-Torrent, M.; Veciana, J.; Rovira, C.; Cornil, J. Design of Perchlorotriphenylmethyl (PTM) Radical-Based Compounds for Optoelectronic Applications: The Role of Orbital Delocalization. *ChemPhysChem* **2018**, *19*, 2572–2578.

(58) Tonnelé, C.; Casanova, D. Rationalization and tuning of doublet emission in organic radicals. *Journal of Materials Chemistry C* **2022**, *10*, 13826–13833.

(59) Shen, T.; Dijkstra, D.; Farrando-Pérez, A.; Boj, P. G.; Villalvilla, J. M.; Quintana, J. A.; Zou, Y.; Hou, X.; Wei, H.; Li, Z. et al. Fused Triangulene Dimers: Facile Synthesis by Intramolecular Radical-Radical Coupling and Application for Near-Infrared Lasers. *Angewandte Chemie International Edition* **2023**, *62*, e202304197.

(60) Ju, C.-W.; Shen, Y.; French, E. J.; Yi, J.; Bi, H.; Tian, A.; Lin, Z. Accurate Electronic and Optical Properties of Organic Doublet Radicals Using Machine Learned Range-Separated Functionals. *The Journal of Physical Chemistry A* **2024**, *128*, 2457–2471.

(61) Su, J.; Telychko, M.; Song, S.; Lu, J. Triangulenes: From Precursor Design to On-Surface Synthesis and Characterization. *Angewandte Chemie International Edition* **2020**, *59*, 7658–7668.

(62) Pariser, R.; Parr, R. G. A Semi-Empirical Theory of the Electronic Spectra and Electronic Structure of Complex Unsaturated Molecules. I. *The Journal of Chemical Physics* **1953**, *21*, 466–471.

(63) Pariser, R.; Parr, R. G. A Semi-Empirical Theory of the Electronic Spectra and Electronic Structure of Complex Unsaturated Molecules. II. *The Journal of Chemical Physics* **1953**, *21*, 767–776.

(64) Pople, J. A. Electron interaction in unsaturated hydrocarbons. *Transactions of the Faraday Society* **1953**, *49*, 1375.

(65) Pariser, R. Theory of the Electronic Spectra and Structure of the Polyacenes and of Alternant Hydrocarbons. *The Journal of Chemical Physics* **1956**, *24*, 250–268.

(66) Pariser, R. Electronic Spectrum and Structure of Azulene. *The Journal of Chemical Physics* **1956**, *25*, 1112–1116.

(67) Favini, G.; Vandoni, I.; Simonetta, M. Calculation of electronic spectra of aza-benzenes and aza-naphthalenes by the Pariser-Parr-Pople method. *Theoretica Chimica Acta* **1965**, *3*, 45–58.

(68) Albert, I. D. L.; Ramasesha, S.; Das, P. K. Properties of some low-lying electronic states in polymethineimines and poly(2,3-diazabutadienes). *Physical Review B* **1991**, *43*, 7013–7019.

(69) Mukhopadhyay, S.; Topham, B. J.; Soos, Z. G.; Ramasesha, S. Neutral and Charged Excited States in Polar Organic Films: Origin of Unusual Electroluminescence in Tri-*p*-tolylamine-Based Hole Conductors. *The Journal of Physical Chemistry A* **2008**, *112*, 7271–7279.

(70) Kumar, M.; Pati, Y. A.; Ramasesha, S. A density matrix renormalization group method study of optical properties of porphines and metalloporphines. *The Journal of Chemical Physics* **2012**, *136*, 014112.

(71) Thomas, S.; Pati, Y.; Ramasesha, S. Linear and nonlinear optical properties of expanded porphyrins: A DMRG study. *The Journal of Physical Chemistry A* **2013**, *117*, 7804–7809.

(72) Aryanpour, K.; Shukla, A.; Mazumdar, S. Electron correlations and two-photon states in polycyclic aromatic hydrocarbon molecules: A peculiar role of geometry. *The Journal of Chemical Physics* **2014**, *140*, 104301.

(73) Bhattacharyya, P.; Rai, D. K.; Shukla, A. Pariser–Parr–Pople Model Based Configuration-Interaction Study of Linear Optical Absorption in Lower-Symmetry Polycyclic Aromatic Hydrocarbon Molecules. *The Journal of Physical Chemistry C* **2020**, *124*, 14297–14305.

(74) Poh, Y. R.; Morozov, D.; Kazmierczak, N. P.; Hadt, R. G.; Groenhof, G.; Yuen-Zhou, J. Alternant Hydrocarbon Diradicals as Optically Addressable Molecular Qubits. *Journal of the American Chemical Society* **2024**, *146*, 15549–15561.

(75) Bedogni, M.; Di Maiolo, F. Singlet-Triplet Inversion in Triangular Boron Carbon Nitrides. 2024; `https://doi.org/10.26434/chemrxiv-2024-glhqn-v2`, Preprint (ChemRxiv), accessed on August 25, 2024.

(76) Hele, T. J. H. On the electronic structure of alternant conjugated organic radicals for light-emitting diode applications. Physical Chemistry of Semiconductor Materials and Interfaces XX. 2021; p 117991A.

(77) Green, J. D.; Hele, T. J. H. ExROPPP: Fast, accurate, and spin-pure calculation of the electronically excited states of organic hydrocarbon radicals. *The Journal of Chemical Physics* **2024**, *160*, 164110.

(78) Ellis, R. L.; Kuehnlenz, G.; Jaffé, H. H. The use of the CNDO method in spectroscopy: VI. further n-$\pi*$ $transitions.Theoretica$ $Chimica$ $Acta$**1972**, *26*, 131 − −140.$Surján$, $P.R.$; $Kuzmany$, $H.Interruptionofconjugationsofpolyacetylenechains.Physical$ Re −2624.

(79) Hele, T. J. H.; Fuemmeler, E. G.; Sanders, S. N.; Kumarasamy, E.; Sfeir, M. Y.; Campos, L. M.; Ananth, N. Anticipating Acene-Based Chromophore Spectra with Molecular Orbital Arguments. *The Journal of Physical Chemistry A* **2019**, *123*, 2527–2536.

(81) Green, J. D.; Fuemmeler, E. G.; Hele, T. J. H. Inverse molecular design from first principles: Tailoring organic chromophore spectra for optoelectronic applications. *The Journal of Chemical Physics* **2022**, *156*.

(82) Radovic, L. R.; Karra, M.; Skokova, K.; Thrower, P. A. The role of substitutional boron in carbon oxidation. *Carbon* **1998**, *36*, 1841–1854.

(83) Perkins, P. G.; Wall, D. H. Self-consistent molecular-orbital calculations on borazines. *Journal of the Chemical Society A: Inorganic, Physical, Theoretical* **1966**, 235.

(84) Jensen, H.; Skancke, P. N.; Westman, S.; Norin, T. Semi-empirical Parameters in pi-Electron Systems. V. The Carbonyl Group. *Acta Chemica Scandinavica* **1968**, *22*, 2899–2909.

(85) Chandra Jha, P.; Krishnan, A.; Das, P. K.; Ramasesha, S. Nonlinear optical properties of linear chain phosphazenes, (PN)x. *The Journal of Chemical Physics* **2002**, *117*, 2873–2881.

(86) Das, M. Low-lying excitations of poly-fused thiophene within Pariser–Parr–Pople model: A density matrix renormalization group study. *The Journal of Chemical Physics* **2010**, *132*.

(87) Coulson, C. A.; Rushbrooke, G. S. Note on the method of molecular orbitals. *Mathematical Proceedings of the Cambridge Philosophical Society* **1940**, *36*, 193–200.

(88) McLachlan, A. The pairing of electronic states in alternant hydrocarbons. *Molecular Physics* **1959**, *2*, 271–284.

(89) Koutecký, J. Contribution to the Theory of Alternant Systems. *The Journal of Chemical Physics* **1966**, *44*, 3702–3706.

(90) Lieb, E. H.; Wu, F. Y. Absence of Mott Transition in an Exact Solution of the Short-Range, One-Band Model in One Dimension. *Physical Review Letters* **1968**, *20*, 1445–1448.

(91) Heilmann, O. J.; Lieb, E. H. VIOLATION OF THE NONCROSSING RULE: THE HUBBARD HAMILTONIAN FOR BENZENE*. *Annals of the New York Academy of Sciences* **1971**, *172*, 584–617.

(92) Laforgue, A.; Čížek, J.; Paldus, J. Study of the correlation effects in a three-electron model system using the projected Hartree-Fock method and the natural spin orbital formalism. *The Journal of Chemical Physics* **1973**, *59*, 2560–2571.

(93) Čížek, J.; Paldus, J.; Hubač, I. Correlation effects in the low–lying excited states of the PPP models of alternant hydrocarbons. I. Qualitative rules for the effect of limited configuration interaction. *International Journal of Quantum Chemistry* **1974**, *8*, 951–970.

(94) Bondeson, S.; Soos, Z. Charge transfer transitions in extended correlated electronic systems. *Chemical Physics* **1979**, *44*, 403–414.

(95) Ducasse, I. R.; Miller, T. E.; Soos, Z. G. Correlated states in finite polyenes: Exact PPP results. *The Journal of Chemical Physics* **1982**, *76*, 4094–4104.

(96) Soos, Z. G. Electronic Structure of Ion-Radical Organic Solids and Polyenes. *Israel Journal of Chemistry* **1983**, *23*, 37–48.

(97) Živković, T. P. Particle-hole symmetry and complementary quantum systems. *International Journal of Quantum Chemistry* **1988**, *34*, 333–359.

(98) Surján, P. R. *Second Quantized Approach to Quantum Chemistry*; Springer Berlin Heidelberg, 1989.

(99) Mallion, R. B.; Rouvray, D. H. The golden jubilee of the Coulson-Rushbrooke pairing theorem. *Journal of Mathematical Chemistry* **1990**, *5*, 1–21.

(100) Misurkin, I. A.; Ovchinnikov, A. A. The Electronic Structure of Conjugated Systems in Terms of the Pariser–Parr–Pole Approximation. *Russian Chemical Reviews* **1974**, *43*, 1072.

(101) Ohno, K. Some remarks on the Pariser-Parr-Pople method. *Theoretica chimica acta* **1964**, *2*, 219–227.

(102) Lehoucq, R.; Sorensen, D.; Yang, C. *ARPACK Users' Guide*; Society for Industrial and Applied Mathematics, 1998.

(103) Lakowicz, J. R. *Principles of fluorescence spectroscopy*, 3rd ed.; Springer: New York, 2006.

(104) Reid, D. Stable -electron systems and new aromatic structures. *Tetrahedron* **1958**, *3*, 339–352.

(105) Gerson, F. Notiz über das ESR.-Spektrum des Phenalenyl-Radikals. *Helvetica Chimica Acta* **1966**, *49*, 1463–1467.

(106) Goto, K.; Kubo, T.; Yamamoto, K.; Nakasuji, K.; Sato, K.; Shiomi, D.; Takui, T.; Kubota, M.; Kobayashi, T.; Yakusi, K. et al. A Stable Neutral Hydrocarbon Radical: Synthesis, Crystal Structure, and Physical Properties of 2,5,8-Tri-tert-butylphenalenyl. *Journal of the American Chemical Society* **1999**, *121*, 1619–1620.

(107) Fukui, K.; Sato, K.; Shiomi, D.; Takui, T.; Itoh, K.; Gotoh, K.; Kubo, T.; Yamamoto, K.; Nakasuji, K.; Naito, A. Electronic structure of a stable phenalenyl radical in crystalline state as studied by SQUID measurements, cw-ESR, and 13C CP/MAS NMR spectroscopy. *Synthetic Metals* **1999**, *103*, 2257–2258.

(108) Itkis, M. E.; Chi, X.; Cordes, A. W.; Haddon, R. C. Magneto-Opto-Electronic Bistability in a Phenalenyl-Based Neutral Radical. *Science* **2002**, *296*, 1443–1445.

(109) Reid, D. H. The chemistry of the phenalenes. *Quarterly Reviews, Chemical Society* **1965**, *19*, 274.

(110) Cofino, W.; van Dam, S.; Kamminga, D.; Hoornweg, G.; Gooijer, C.; MacLean, C.; Velthorst, N. Jahn-Teller effect in highly resolved optical spectra of the phenalenyl radical. *Molecular Physics* **1984**, *51*, 537–550.

(111) Zheng, S.; Lan, J.; Khan, S. I.; Rubin, Y. Synthesis, Characterization, and Coordination Chemistry of the 2-Azaphenalenyl Radical. *Journal of the American Chemical Society* **2003**, *125*, 5786–5791.

(112) Morita, Y.; Aoki, T.; Fukui, K.; Nakazawa, S.; Tamaki, K.; Suzuki, S.; Fuyuhiro, A.; Yamamoto, K.; Sato, K.; Shiomi, D. et al. A New Trend in Phenalenyl Chemistry: A Persistent Neutral Radical, 2,5,8-Tri-tert-butyl-1,3-diazaphenalenyl, and the Excited Triplet State of the Gablesyn-Dimer in the Crystal of Column Motif. *Angewandte Chemie International Edition* **2002**, *41*, 1793–1796.

(113) Zheng, S.; Thompson, J. D.; Tontcheva, A.; Khan, S. I.; Rubin, Y. Perchloro-2,5,8-triazaphenalenyl Radical. *Organic Letters* **2005**, *7*, 1861–1863.

(114) Suzuki, S.; Morita, Y.; Fukui, K.; Sato, K.; Shiomi, D.; Takui, T.; Nakasuji, K. Hexaazaphenalenyl Anion Revisited: A Highly Symmetric Planar System with Multiple-Networking Ability for Self-Assembled Metal Complexation. *Inorganic Chemistry* **2005**, *44*, 8197–8199.

(115) Ito, S. The Rapid Synthesis of -Extended Azacorannulenes. *Journal of Synthetic Organic Chemistry, Japan* **2019**, *77*, 1128–1135.

(116) Soos, Z. G.; Ramasesha, S. Valence-bond theory of linear Hubbard and Pariser-Parr-Pople models. *Physical Review B* **1984**, *29*, 5410–5422.

(117) Prodhan, S.; Soos, Z. G.; Ramasesha, S. Model for triplet state engineering in organic light emitting diodes. *The Journal of Chemical Physics* **2014**, *140*, 214313.

(118) Nishimoto, K.; Forster, L. S. SCFMO calculations of heteroatomic systems with the variable? approximation. *Theoretica Chimica Acta* **1966**, *4*, 155–165.

(119) Michl, J.; Koutecky, J.; Becker, R. S.; Earhart, C. E. A note on the parameters for heteroatoms in Pariser-Parr-Pople (PPP) calculations. *Theoretica Chimica Acta* **1970**, *19*, 92–97.

(120) Hinze, J.; Beveridge, D. L. Parametrization of semiempirical π-electron molecular orbital calculations. π Systems containing carbon, nitrogen, oxygen, and fluorine. *Journal of the American Chemical Society* **1971**, *93*, 3107–3114.

(121) Zahradník, R.; Tesařová, I.; Pancíř, J. Experimental and theoretical (HMO and LCI-SCF) study of singlet-triplet transitions in conjugated hydrocarbons and their derivatives. *Collection of Czechoslovak Chemical Communications* **1971**, *36*, 2867–2880.

(122) Griffiths, J. Practical aspects of colour prediction of organic dye molecules. *Dyes and Pigments* **1982**, *3*, 211–233.

(123) Grossjean, M. F.; Tavan, P. Wavelength regulation in bacteriorhodopsin and halorhodopsin: A Pariser–Parr–Pople multireference double excitation configuration interaction study of retinal dyes. *The Journal of Chemical Physics* **1988**, *88*, 4884–4896.

(124) Albert, I. D. L.; Das, P. K.; Ramasesha, S. Optical nonlinearities in symmetric cyanine dyes and related systems. *Journal of the Optical Society of America B* **1993**, *10*, 1365.

(125) Maurice, D.; Head-Gordon, M. On the Nature of Electronic Transitions in Radicals: An Extended Single Excitation Configuration Interaction Method. *The Journal of Physical Chemistry* **1996**, *100*, 6131–6137.

(126) Ramasesha, S.; Soos, Z. Magnetic and optical properties of exact PPP states of naphthalene. *Chemical Physics* **1984**, *91*, 35–42.

(127) Scriven, E.; Powell, B. J. Toward the parametrization of the Hubbard model for salts of bis(ethylenedithio)tetrathiafulvalene: A density functional study of isolated molecules. *The Journal of Chemical Physics* **2009**, *130*, 104508.

(128) Di Maiolo, F.; Masino, M.; Painelli, A. Terahertz-pulse driven modulation of electronic spectra: Modeling electron-phonon coupling in charge-transfer crystals. *Physical Review B* **2017**, *96*, 075106.

(129) Frisch, M. J.; Trucks, G. W.; Schlegel, H. B.; Scuseria, G. E.; Robb, M. A.; Cheeseman, J. R.; Scalmani, G.; Barone, V.; Petersson, G. A.; Nakatsuji, H. et al. Gaussian˜16 Revision B.01. 2016; Gaussian Inc. Wallingford CT.

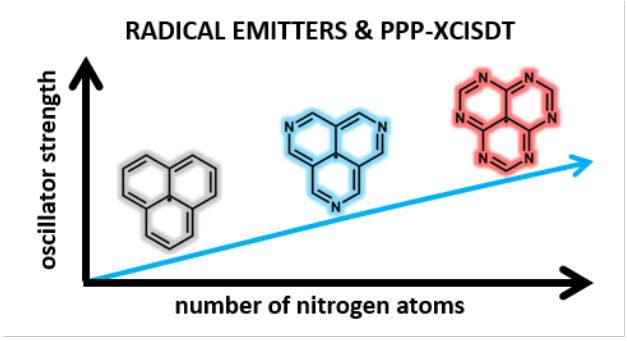

Figure 7: TOC Graphic